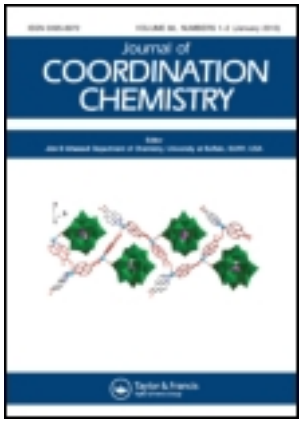

Journal of Coordination Chemistry
Publication details, including instructions for authors and subscription information:
http://www.tandfonline.com/loi/gcoo20

DNA binding, nuclease, and colon cancer cell inhibitory activity of a Cu(II) complex of a thiazolidine-4-carboxylic acid derivative

S. Thalamuthu [a] , B. Annaraj [a] , Smreti Vasudevan [b] , Suparna Sengupta [b] & M.A. Neelakantan [a]

[a] Chemistry Research Centre, National Engineering College , Kovilpatti , India

[b] Cancer Research Program-3, Rajiv Gandhi Centre for Biotechnology , Trivandrum , India

Accepted author version posted online: 03 Apr 2013.Published online: 02 May 2013.

To cite this article: S. Thalamuthu , B. Annaraj , Smreti Vasudevan , Suparna Sengupta & M.A. Neelakantan (2013) DNA binding, nuclease, and colon cancer cell inhibitory activity of a Cu(II) complex of a thiazolidine-4-carboxylic acid derivative, Journal of Coordination Chemistry, 66:10, 1805-1820, DOI: 10.1080/00958972.2013.791393

To link to this article: http://dx.doi.org/10.1080/00958972.2013.791393

Journal of Coordination Chemistry, 2013
Vol. 66, No. 10, 1805–1820, http://dx.doi.org/10.1080/00958972.2013.791393

DNA binding, nuclease, and colon cancer cell inhibitory activity of a Cu(II) complex of a thiazolidine-4-carboxylic acid derivative

S. THALAMUTHU†, B. ANNARAJ†, SMRETI VASUDEVAN‡, SUPARNA SENGUPTA‡ and M.A. NEELAKANTAN*†

†Chemistry Research Centre, National Engineering College, Kovilpatti, India
‡Cancer Research Program-3, Rajiv Gandhi Centre for Biotechnology, Trivandrum, India

(*Received 13 July 2012; in final form 17 January 2013*)

Thiazolidine-4-carboxylic acid derivative (L) derived by condensation of D-penicillamine and 3-methoxy salicylaldehyde was used in synthesis of a copper complex (CuL). The ligand and Cu (II) complex were characterized by elemental analysis and spectral techniques. The DNA binding properties of L and CuL with calf thymus DNA were investigated by various techniques. The ability of compounds to break pUC19 DNA was checked by gel electrophoresis. The radical-scavenging activity was studied using 2,2-diphenyl-1-picrylhydrazyl assay. The ligand and CuL exert cytotoxicity against HCT116 cell line. The compounds were screened for antimicrobial activity against several microorganisms. The effect of the CuL on the surface of penicillium was analyzed by scanning electron microscopy.

Keywords: Thiazolidine-4-carboxylic acid derivative; Copper complex; Spectral studies; Biological activity

1. Introduction

Thiazolidines are an important class of S, N-containing heterocycles present in a great number of substances with biological properties. Compounds possessing a thiazolidine ring are potent enzyme inhibitors and receptor antagonists. These compounds have interest as potential antibiotic and antitumor agents. Some thiazoline derivatives have interesting anti-HIV or anticancer activities and can inhibit cell division [1]. Thiazolidine-4-carboxylic acid and its derivatives induce the restoration of "contact inhibition" to tumor cells and its interaction with metal ions seems to be of critical importance [2–4]. Thus, thiazolidines are important building blocks in pharmaceutical agents [5–7]. The reaction between 1,2-aminothiols and aldehydes deserves attention as it is associated with many biochemical processes and involves cyclization by condensation, leading to the formation of cyclic thiazoline or thiazolidine derivatives [8]. The biological activity of thiazolidines could be modified or even improved when coordinated to metal ions [9]. The thiazoline ring is present in the structure of bacitracin A, a broad spectrum antibiotic whose activity is improved through coordination to Zn(II) [10]. Cu(II) is one of the most relevant transition metal ions

*Corresponding author. Email: hodsh@nec.edu.in

with biological properties, performing several diverse functions including transport of oxygen and electrons, catalysis in oxidation reduction reactions and protection of the cell against damaging oxygen radicals [11].

This aroused our interest to synthesize a thiazolidine-4-carboxylic acid derivative and its copper complex (CuL). The thiazolidine-4-carboxylic acid derivative (L) derived by the condensation of D-penicillamine and 3-methoxy salicylaldehyde was used in the synthesis of CuL. These compounds were evaluated for binding behavior with calf thymus DNA (CT-DNA) using spectral and kinetic techniques. The DNA cleaving nature of the compounds was tested against pUC19 DNA in the absence and presence of hydrogen peroxide. The *in vitro* biological activity of the compounds was assessed against various microorganisms. The effect of the complex on the surface of the penicillium fungus has been analyzed by scanning electron microscopy (SEM). The antioxidant and anticancer activities of the compounds were also experimentally explored.

2. Experimental

2.1. *Materials and methods*

D-penicillamine, 3-methoxy salicylaldehyde, and copper perchlorates were purchased from Aldrich and used without purification. All other reagents were procured from commercial sources. Doubly distilled water was used in the preparation of all the solutions. CT DNA and pUC19 DNA were purchased from Genei, India, and stock solutions were prepared in Tris–HCl buffer solution (50 mM Tris–HCl, 18 mM NaCl, pH 7.2) and kept frozen. Agarose (molecular biology grade) and ethidium bromide (EB) were purchased from Sigma. Solvents for spectroscopic and electrochemical studies were purified and dried by standard procedures [12]. The elemental analysis was performed using an Elementar Model Vario EL III analyzer. The molar conductance of CuL in DMSO was measured using a Systronics 304 conductivity bridge. IR spectra were recorded with samples as KBr pellets in a Shimadzu FTIR-8400S spectrophotometer. ^{1}H NMR spectra were recorded in DMSO-d_6 on a Bruker AMX 400 MHz spectrometer using TMS as reference. Electronic spectra were obtained on a Shimadzu UV–vis 2450 spectrophotometer. ESI mass spectra of the ligand and its CuL were recorded on a Bruker Daltonics esquire 4000 MS system. The X-band EPR spectra of the Cu (II) complex in DMSO at room temperature and liquid nitrogen conditions were obtained on a Varian EPR spectrometer. The thermogram of the CuL was recorded in dynamic nitrogen with a heating rate of 20 °C/min using a SDT Q600 V8.3 Build 101 thermal analyzer. The fluorescence spectra were recorded on a Shimadzu RF-5301PC spectrofluorophotometer. Cyclic voltammetric studies on the CuL in buffer solution containing 5% DMSO were carried out at room temperature using a CHI 603C electrochemical analyzer. The effect of the CuL on the surface of the penicillium fungus was studied by SEM (LEO 435 VP) at 25 kV Voltage. Ninety-six well plates were from Corning and 3-(4,5-dimethyl-2-thiazolyl)-2,5-diphenyltetrazolium bromide (MTT) was from USB, USA.

2.2. *Synthesis*

2.2.1. Synthesis of L. D-penicillamine (0.1491 g, 1.0 mM) and 3-methoxy salicylaldehyde (0.1522 g, 1.0 mM) in 50% methanol/water (30 mL) were refluxed for two hours. The resulting solution was reduced to one third of its original volume, and cooled to room temperature.

The solution was kept at room temperature closed condition for a day. Colorless crystals were collected by filtration, washed with chloroform, and dried under vacuum. The product was recrystallized with 50% methanol water mixture. Anal. Calcd for $C_{13}H_{17}NO_4S$ (%): C, 55.11; H, 6.05; N, 4.94; S, 11.32. Found (%): C, 55.32; H, 6.24; N, 5.01; S, 11.45. IR data (KBr, cm^{-1}): (s = strong, m = medium, b = broad). 3400–2700 (b) [ν(OH)]; 1635 (s) [$\nu_{asym}(COO^-)$], 1369 (s) [$\nu_{sym}(COO^-)$]; 1354 (m) [δ(OH)]; 1247 (s) [ν(C–O)]; 833 (w) [ν(C–S–C)]; ^{1}H NMR (400 MHz, DMSO-d6, ppm): 1.62 (singlet (s), CH_3, 3H), 1.31 (singlet (s), CH_3, 3H), 3.38 (singlet, –CH–COOH, 1H), 6.69–6.92 (multiplet, aromatic H, 3H), 3.84 (singlet, 3H, OCH_3), 5.79 (singlet, thiazolidine –CH–NH, 1H). Color: white. M.p. 143 °C; Yield: 73%.

2.2.2. Synthesis of CuL. L (0.281 g, 1.0 mM) in 10 mL methanol was added dropwise to $Cu(ClO_4)_2 \cdot 6H_2O$ (0.1705 g) in 10 mL methanol and the mixture was refluxed for 2 h. The pH of the solution was adjusted to five using 0.01 M KOH solution. The resulting solution was reduced to one third of its volume and cooled to room temperature. CuL was precipitated as green powder, thoroughly washed with water followed by acetone, and dried under vacuum. The perchlorate salts of metals are explosive, a small quantity of the sample was used with necessary precautions. The synthetic scheme of ligand and its CuL is given in scheme 1.

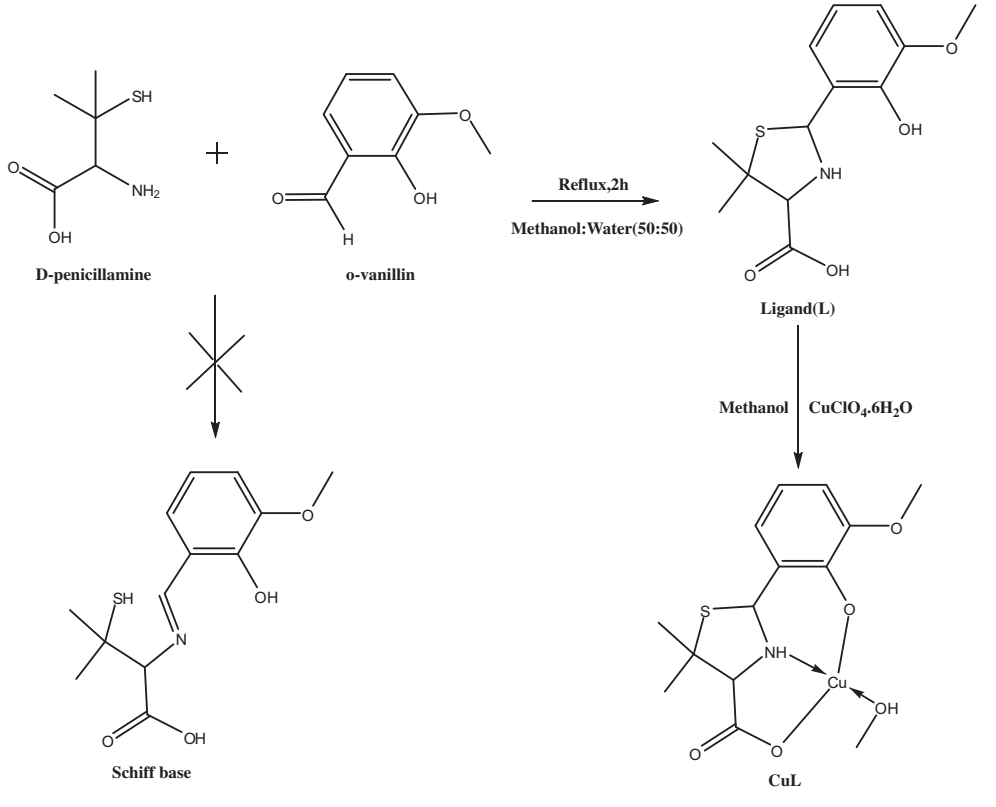

Scheme 1. Synthesis of L and CuL.

CuL complex: Anal. Calcd for $[Cu(C_{13}H_{15}NO_4S)(CH_3OH)]\cdot H_2O$ (%): Cu, 16.09; C, 42.58; H, 5.36; N, 3.55; S, 8.12. Found (%): Cu, 16.15; C, 42.66; H, 5.45; N, 3.68; S, 8.21. IR data (KBr, cm^{-1}): (s = strong, m = medium, b = broad). 3400–3020 (b) [ν(OH)], 1604 (s) [$\nu_{asym}(COO^-)$], 1384 (m) [$\nu_{sym}(COO^-)$], 1585 (s) [ν(C=C)], 1268 (s) [ν(C–O)], 840 (w) [ν(C–S)], 476 (w) [ν(M–O)], 528 (w) [ν(M–N)]. Color: green. M.p. 290 °C; Yield: 71%. Λ_m, 8 mho M^{-1} cm^2.

2.3. *DNA binding studies*

DNA-binding nature of L and CuL was studied using absorption spectroscopy, fluorescence spectroscopy, cyclic voltammetry, viscosity, and thermal denaturation methods.

2.3.1. Absorption spectral studies. Electronic absorption spectral studies were used to study the binding of L and CuL with DNA. CT DNA was deproteinized with sodium dodecyl sulfate (SDS, protein content less than 0.2%) and extensively dialyzed against the Tris–HCl buffer solution (pH = 7.2) until the UV absorbance ratio A_{260}/A_{280} was greater than 1.86. The concentration of the prepared CT DNA stock solution was determined according to its absorbance at 260 nm using $\varepsilon_{260} = 6600\ M^{-1}\ cm^{-1}$. Stock solution of DNA was stored at 4 °C and used within seven days. Absorption titration experiments were done using fixed concentration of compounds (40 μM) and varying the concentration of the CT DNA (10–50 μM). While measuring the spectra, an equal amount of DNA was added to both the compound and reference solutions to eliminate the absorbance of DNA itself. The intrinsic binding constant, K_b, was determined by the following equation (1), [13]

$$\frac{[DNA]}{(\varepsilon_a - \varepsilon_f)} = \frac{[DNA]}{(\varepsilon_b - \varepsilon_f)} + \frac{1}{K_b(\varepsilon_b - \varepsilon_f)} \quad (1)$$

where ε_a ε_f, and ε_b are the extinction coefficients of the apparent, free and bound CuL, respectively.

2.3.2. Fluorescence spectral studies. The interactions of L and CuL with DNA were studied by fluorescence spectral method using EB-bound CT DNA in Tris–HCl/NaCl buffer solution (pH 7.2). The excitation wavelength was fixed at 545 nm and the emission range was adjusted before measurements. Changes in the fluorescence intensities at 617 nm of EB (25 μM) bound CT DNA (10 μM) in Tris HCl buffer (pH 7.2) were measured with respect to different concentrations of the compounds (10–50 μM). The magnitude of the binding strength of the compounds with CT DNA can be calculated using the linear Stern–Volmer equation (2) [14]

$$\frac{I_0}{I} = 1 + K_{SV}[Q] \quad (2)$$

where I_0 and I represent the fluorescence intensities of EB-DNA in the absence and presence of quencher, respectively. Q is the concentration of the metal complex. K_{sv} is the linear Stern–Volmer quenching constant. The relative binding tendency of the complex to CT DNA was determined by comparison of the slope of the line in the fluorescence intensity

versus complex concentration. The apparent binding constant (K_{app}) was calculated using the equation $K_{app} = K_{EB}[EB]/[complex]$, where [complex] is the concentration of the complex at which there is 50% reduction in the fluorescence intensity of EB, $K_{EB} = 1.0 \times 10^7$ M^{-1} and [EB] = 25 μM [15].

2.3.3. Melting temperature. DNA melting experiments were carried out by monitoring the absorption intensity of CT DNA (200 μM) at 260 nm at various temperatures in the presence and absence of L and CuL (40 μM), respectively. Measurements were carried out on a Shimadzu UV/VIS 2450 spectrophotometer equipped with a Cyberlab constant temperature water bath (CB 2000 V) on increasing the temperature of the solution at 1°C per min.

2.3.4. Viscosity measurements. Viscosity measurements were carried out on an Ostwald-type viscometer, thermostated in a water bath maintained at 30 ± 1 °C. The viscosity for DNA was measured in the presence and absence of L and CuL, respectively. The flow time of DNA (200 μM) was monitored by varying the complex concentration (20–200 μM). Flow time of each sample was measured three times with a digital stopwatch, and an average flow time was used. The relative viscosities for DNA in the presence (η) and absence (η_o) of the complex were calculated using the relation $\eta = (t - t^o)/t^o$, where t and t^o are the observed flow time for each sample and buffer, respectively. The values of the relative viscosity $(\eta/\eta_o)^{1/3}$ were plotted against [complex]/[DNA].

2.3.5. Cyclic voltammetry. Cyclic voltammetry experiments for L and CuL were performed in DMSO solution at ambient temperature (27 °C) within the potential range +1.0 to −1.25 V using glassy carbon as the working electrode, a platinum coil as auxiliary electrode and Ag/AgCl as the reference electrode in the process. The supporting electrolyte was 0.05 M tetrabutylammonium perchlorate in DMSO solution. The cell was maintained oxygen free by passing dry nitrogen through the solution. Interaction of the CuL with CT DNA was investigated by monitoring the changes observed in the cyclic voltammogram of CuL in Tris–HCl buffer with increasing amounts of DNA.

2.4. *Nuclease activity*

DNA cleavage of L and CuL were monitored using agarose gel electrophoresis. Supercoiled pUC19 DNA (100 μM) in 5% DMSO and 95% Tris buffer (5 mM, 50 mM NaCl, pH 7.2) was treated with L and CuL in the presence and absence of hydrogen peroxide as activator. The reaction mixture (DNA, L/CuL, H_2O_2 and sufficient buffer) was incubated at 37 °C followed by addition of loading buffer containing 0.25% bromophenol blue, 50% glycerol and 0.61% Tris buffer. The solution was finally loaded on 1% agarose gel containing 0.5 μg mL^{-1} EB. Electrophoresis was performed for 2 h at 50 V. Bands were visualized by photographing the fluorescence of intercalated EB under a UV illuminator.

2.5. *Measurement of antioxidant activity*

Stock solution of DPPH (2,2-diphenyl-1-picrylhydrazyl) was prepared by dissolving 0.2 mg of DPPH in 1 mL of methanol. The ligand or its CuL (0.05–0.25 mg mL^{-1}) was mixed with the DPPH solution (500 μM) and the mixture was kept at room temperature

for 30 min. The absorbance of the resulting solution was measured at 517 nm using a UV-vis Shimadzu 2450 spectrophotometer. The radical scavenging capacity of antioxidants was expressed as percentage inhibition and IC_{50}. The IC_{50} value is the concentration of the antioxidant required to scavenge 50% DPPH radical and it is calculated from the inhibition curve.

2.6. *Cytotoxicity assay by MTT*

The MTT assay was used to determine cell viability as an indicator, for the sensitivity of the cells to the ligand and its CuL. HCT116 cells were seeded on 96 well tissue-culture treated polystyrene, flat bottom plates with cell density of 3000 cells/well. The compounds were dissolved in DMSO and tested with concentrations ranging from 0.5–50 μM. The different concentrations of L and CuL were added into the cells in quadruplicates. After 48 h incubation, media were discarded, given a PBS wash. The formazan crystals formed were dissolved in 100 μL lysis buffer (50% dimethylformamide and 20% SDS). Optical density of the solution was measured at 570 nm using a Bio-Rad Model 680 microplate reader. Data were collected for four replicates each and used to calculate the mean. The inhibitory concentration (IC_{50}) was calculated using the nonlinear regression program Origin. 4-Amino-5-benzoyl-2-(4-methoxyphenylamino)thiazole (DAT1) was used as control [16].

2.7. *Antimicrobial activity*

2.7.1. Microorganisms. Bacterial strains: *Escherichia coli*, *Vibrio cholerae*, *Pseudomonas aeruginosa*, and *Salmonella Typhi*. Control: Amoxicillin and Ampicillin. Fungal strains: *A. Niger, Trichoderma harzianum* and *penicillium* sps. *Yeast*: *Saccharomycies*. Control: *Nystatin*.

2.7.2. Antibacterial studies. The antibacterial activities of L and CuL were determined by well plate method in Mueller–Hinton Agar [17]. The *in vitro* antibacterial activity was carried out against 24 h cultures of bacterial strains. Stock solutions of tested compounds were prepared in DMSO to a final concentration of 10 mg mL^{-1}. 20 mL of sterilized agar media was poured into each pre-sterilized Petri dish and allowed to solidify by placing it in an incubator at 37 °C for an hour. After 24 h, culture suspension was poured and neatly swabbed with pre-sterilized cotton swabs. Then holes of 5 mm diameter were punched carefully using a sterile cork borer and these wells were completely filled with the prepared L, or CuL solutions (50 μL). These dishes were transferred to an incubator maintained at 37 °C for 24 h. The antibacterial activity was measured by the diameter of the clear zone, which appeared around the wells in each plate. Experiments were performed in triplicate, and the standard deviation was calculated.

2.7.3. Antifungal and yeast studies. The *in vitro* antifungal and yeast activity of L and CuL were studied by agar well plate method using Sabourands agar media [18]. The antifungal activity was measured by the diameter of the clear zone at the time interval of 24, 48, and 72 h, which appeared around the wells in each plate. Experiments were performed in triplicate and the standard deviation was calculated.

2.7.4. SEM. The effect of the CuL on the surface of penicillium fungi was studied by SEM (LEO 435 VP) at 25 kV comparing the surface morphology penicillium before and after treatment with the CuL. The images have a characteristic three-dimensional (3-D) appearance and are useful for judging the surface of the penicillium sps cell. The cells with a density of 10^8–10^9 cells mL^{-1} were harvested in both the CuL treated and untreated penicillium. The cell pellet was washed with phosphate buffer saline (PBS) thrice followed by resuspension in 1 mL of fixative solution (2.5% gluteraldehyde and 2% formaldehyde) and kept for 6 h at 4 °C. The fixative solution was removed by centrifugation and the cell pellet was washed with PBS several times and finally re-suspended in 1 mL of sodium phosphate buffer. The samples were coated with a nanometer thick layer of gold after mounting them on studs after smearing on glass cover slips and then analyzed by SEM. Images were taken in 500x magnifications.

3. Results and discussion

L and CuL were air stable. The ligand is soluble in methanol, acetone, acetonitrile, DMF, and DMSO, whereas the complex is soluble only in DMF and DMSO. Analytical data and mass spectrum of CuL correspond with the formula CuL. The monomeric nature of the complex was confirmed from its magnetic moment. The low molar conductance indicates a non-electrolyte [19].

3.1. *FTIR spectra*

The formation of a thiazolidine derivative by the condensation of D-penicillamine and o-vanillin is evidenced from the absorption at 833 cm^{-1} (υC–S–C) (figure S1). This band has no change in CuL, suggesting that thiazolidine sulfur of L is free from complexation (table S1). The medium absorption at 1354 cm^{-1} due to in-plane OH bending of the phenol of L disappears in CuL, indicating that phenolic OH is involved in coordination with copper after deprotonation, further confirmed by shift of the phenolic C–O stretch of L at 1247–1268 cm^{-1} in CuL. The ligand shows bands at 1635 cm^{-1} and 1369 cm^{-1}, attributed to $\nu(COO^-)_{asym}$ and $\nu(COO^-)_{sym}$ of carboxylate, respectively. These bands are at 1604 and 1384 cm^{-1} in CuL. The magnitude of separation between these two vibrations (220 cm^{-1}) suggests unidentate coordination of carboxylate [20]. A broad band at 3400–3020 cm^{-1} suggests the presence of lattice waters in the complex, further confirmed by TGA analysis. New bands at 528 and 476 cm^{-1} in the complex are attributed to $\nu_{(M–N)}$ and $\nu_{(M–O)}$ vibrations, respectively [21].

3.2. *^{1}H and ^{13}C NMR spectra*

The ^{1}H NMR spectrum of L does not give a signal for azomethine or –SH, indicating the formation of the thiazolidine ring. Figure S2 shows two sets of signals for each proton due to the presence of two isomers with a ratio of 3:2. The two diastereomers arise from two chiral centers at the thiazolidine ring (C2 and C4). The chemical shifts were much different for C2–H in the thiazolidine ring of the two diastereomers, which could be understood by considering the C2–H signals at 5.79 and 5.90 ppm for the two isomers [22]. The downfield signal at 5.90 ppm is due to the minor isomer. The C4–H signal of the major isomer is at 3.60 ppm, while that of the minor isomer appeared at 3.64 ppm. The signals at

3.85 and 3.77 ppm are attributed to methoxy of the major and minor isomers, respectively. The major isomer gives two methyl signals at 1.62 and 1.32 ppm of which 1.62 ppm corresponds to the methyl *trans* to the carboxylic acid group, and 1.32 ppm corresponds to the methyl *cis* to the carboxylic acid group. Similarly, the minor isomer also gives two methyl signals at 1.47 and 1.26 ppm. The aromatic protons give signals at 6.69–6.93 ppm with intensity equal to five protons, of which three are for the major isomer and two for the minor isomer. The ^{13}C NMR spectrum obtained for L in DMSO-d_6 also supports the formation of the cyclization product (figure S3).

3.3. *Electronic spectra*

Electronic spectra of L and CuL were recorded in DMSO (figure S4). The ligand shows a band at 283 nm corresponding to the $\pi-\pi^*$ transition of the aromatic ring (table S2). This band undergoes a slight bathochromic shift with hypochromism during complexation and a new band arises at 385 nm in the spectrum of the complex, indicating that L forms a complex with copper. The band at 385 nm ($\varepsilon_{max} = 1220\,M^{-1}\ cm^{-1}$) may be assigned to a ligand-to-metal charge transfer transition originating from p_π of the phenolate oxygen to empty d orbitals of the metal [23]. For square-planar complexes with a $d_{x^2-y^2}$ ground state, three spin-allowed transitions are expected viz. $^2B_{1g}\rightarrow{}^2B_{2g}$ ($d_{x^2-y^2} \rightarrow d_{xy}$), $^2B_{1g}\rightarrow{}^2A_{2g}$ ($d_{x^2-y^2} \rightarrow d_z^2$), and $^2B_{1g}\rightarrow{}^2E_g$($d_{x^2-y^2} \rightarrow d_{xz,yz}$) [24]. As these bands are very close in energy, individual transfers cannot be distinguished. In the present work, the d-d transition appears as a broad band centered at 617 nm with an absorption coefficient of 750 $M^{-1}\ cm^{-1}$. This indicates that copper exists as a distorted square planar NO_3 coordination sphere [25, 26].

3.4. *Mass spectra*

Mass spectra of the ligand and the complex were compared for their compositions (figure S5). The ligand shows a peak at 284.3 m/z which is equal to its molecular mass. The CuL shows a molecular ion peak at $m/z = 377.1$, which corresponds to the solvated (coordinated methanol) CuL. The presence of coordinated methanol is also confirmed by thermogravimetric analysis. The solvent-free CuL is detected at $m/z = 345.2$. The fragmentation peaks for the CuL show two peaks at $m/z = 312.3$ and 271. The molecular ion and fragmentation peaks have half intensity peaks due to isotopic distributions of copper (^{63}Cu and ^{65}Cu) [27, 28]. The mass spectra of the ligand and its CuL are in good agreement with their proposed structure.

3.5. *EPR spectra*

In the solid state, the spectrum of CuL shows one absorption peak. In low field, the complex in frozen DMSO (77 K) shows three well resolved peaks out of four peaks. This corresponds to the hyperfine splitting (figure S6) of the copper nucleus (I = 3/2). The fourth component is masked by the broad perpendicular component; hyperfine lines are not resolved in the "perpendicular" region. The spin Hamiltonian parameters of CuL are given in table 1. The magnetic moment value (1.85 B.M.) calculated from the equation $\mu_{eff} = g[s(s+1)]^{1/2}$ using the experimental g_{iso} values (2.14) agrees very well with the measured value of 1.98 B.M., indicating that the solid structure is retained in DMSO solution. The magnetic moment value obtained (1.98 B.M.) corresponding to one unpaired electron indicates that the complex is mononuclear. This is also evident from the absence of a half field

Table 1. Spin-Hamiltonian parameters of CuL in DMSO at 300 and 77 K.

	Hyperfine constant $\times 10^{-4}$ (cm^{-1})										
Complex	$K_{\parallel}$	$K_{\perp}$	g_{iso}	$A_{\parallel}$	$A_{\perp}$	$g_{\parallel}$	$g_{\perp}$	α^2	β^2	γ^2	$g_{\parallel}/A_{\parallel}$
CuL	0.65	0.47	2.14	163	140	2.27	2.05	0.78	0.84	0.60	139

signal at 1600 G due to the $m_s = \pm 2$ transitions ruling out Cu–Cu interaction. The exchange interaction term G [$G = (g_{\parallel} - 2.0036)/(g_{\perp} - 2.0036)$] observed for the Cu(II) complex ($G = 5.6$) suggests that the exchange coupling effects are not operative in the present complex. The $g_{\parallel}$ and $g_{\perp}$ values were computed from the spectrum using DPPH free radical as g-marker. The $g_{\parallel} > g_{\perp}$ accounts for the distorted square planar structure and rules out the possibility of a trigonal bipyramidal structure, which would be expected to have $g_{\perp} > g_{\parallel}$. The trend of $g_{\parallel} > g_{\perp} > g_e$ observed in the complex shows that the unpaired electron lies predominantly in the $d_{x^2-y^2}$ orbital with Cu(II) having $^2B_{1g}$ as the ground state. The covalency parameter α^2 is calculated using the following equation (3):

$$\alpha^2 = -(A_{\parallel}/0.036) + (g_{\parallel} - 2.0036) + 3/7(g_{\perp} - 2.0036) + 0.04 \quad (3)$$

The observed α^2 value of 0.78 indicates covalent character of the complex in the ligand environment.

3.6. *Thermal analysis*

The TG/DTG curve of the CuL is shown in figure S7 and the data of the main decomposition stages are given in table 2. The complex decomposes in four stages. In the first stage (to 125 °C), there is loss of lattice water (mass loss of 5%). In the second stage, mass loss of 19.82% in 125–180 °C corresponds to loss of a coordinated methanol and decomposition of the thiazolidine part of the ligand with liberation of carbon dioxide. From 180–395 °C, the CuL undergoes decomposition with mass loss of 27.12%, due to loss of the remaining portion of the thiazolidine ring with liberation of hydrogen sulfide. The aromatic part of the ligand decomposed at 395–850 °C and yields copper oxide as the final residue.

3.7. *DNA binding*

3.7.1. Electronic absorption titrations. The potential binding ability of L and CuL to CT DNA was studied by UV–vis spectroscopy. Typical titration curves for L and CuL are shown in figure 1 and the results are reported in table 3. L shows an intense band at

Table 2. Thermal decomposition data of CuL.

			Weight loss	
Compound	Temperature range (°C)	Removed species	Calcd.%	Found%
CuL $[Cu(C_{13}H_{15}NO_4S)(CH_3OH)]\cdot H_2O$	Up to 125	$-H_2O$	4.57	4.72
	125–180	$-CO_2$, $-CH_3OH$	19.24	19.82
	180–395	$-C_4H_{10}OS$ ($-CH_4$, $-H_2S$, $-CH_3OH$)	26.83	27.12
	395–850	$-C_8H_5N$ (aromatic ring)	29.11	30.08

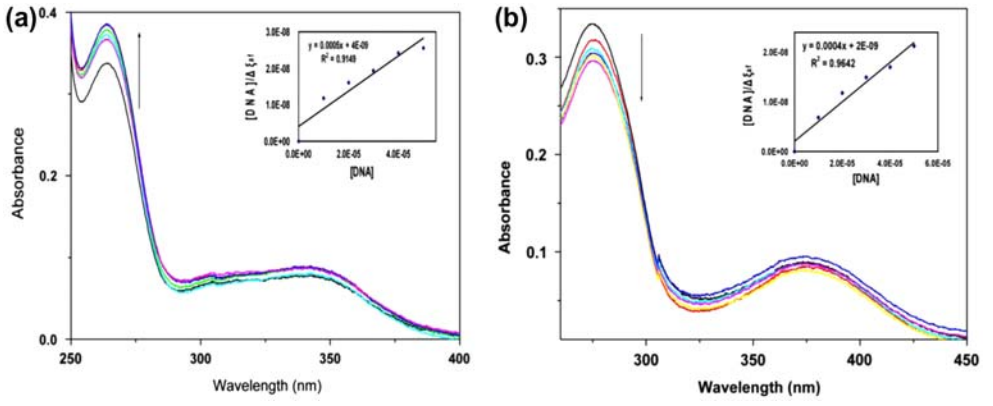

Figure 1. The change in absorbance of (a) L and (b) CuL in the presence of DNA. Arrows show the change of absorbance upon increasing amounts of CT-DNA (10–50 μM) at room temperature.

Table 3. Absorption and emission spectral properties of L and CuL with CT DNA.

	Electronic spectra				Fluorescence spectra		
Compound	λ_{max}	Change in absorbance	Bathochromic shift (nm)	K_b (M^{-1})	λ_{max}	K_{app}	K_{sv} (M^{-1})
L	268	Hyperchromism	–	1.25×10^5	617	–	1.52×10^4
CuL	274	Hypochromism	5	2.0×10^5	617	5.0×10^6	2.5×10^4

268 nm in buffer solution attributed to a $\pi \rightarrow \pi^*$ transition. Upon increasing the CT DNA concentration, hyperchromism is observed, however, there is no change in position of the absorptions. This suggests groove binding between L and DNA. The minor groove contains primarily H-bond acceptor groups, the purine N(3) and pyrimidine O(2) at the floor of the groove walls [29]. The thiazolidine ring of L contains an uncoordinated –NH– which may involve secondary interactions like H-bonding with DNA. The binding constant of L ($K_b = 1.25 \times 10^5$) agrees well with that of the reported minor groove binders [30]. Any interaction between the metal complex and DNA is expected to perturb the ligand-centered transitions of the complex. CuL shows an intense band at 274 nm. Upon increasing the CT DNA concentration, hypochromism and bathochromism are observed in this band, which demonstrates that CuL binds DNA through intercalation. During intercalation, the $\pi \rightarrow \pi^*$ orbital of the complex can couple with the π orbital of the DNA base pairs. This stabilizes the structure of DNA duplex and leads to a decrease in the transition energy of the complex (bathochromic shift). Intercalation may also be due to the insertion of the square planar CuL between the DNA base pairs. This type of atypical intercalation (intercalation with non-fused ring systems) decreases the DNA helical twist and lengthening of the DNA [31, 32]. The K_b value determined for CuL ($K_b = 2.0 \times 10^5$ M^{-1}) agrees well with binding constant values reported for square planar CuLes involved in intercalation with CT DNA [33–35].

3.7.2. Fluorescence spectral studies. In order to substantiate the interaction mode between CT DNA and L/CuL, EB, fluorescence displacement experiments were also carried out. In the absence of CT DNA, EB shows less fluorescence intensity in Tris buffer

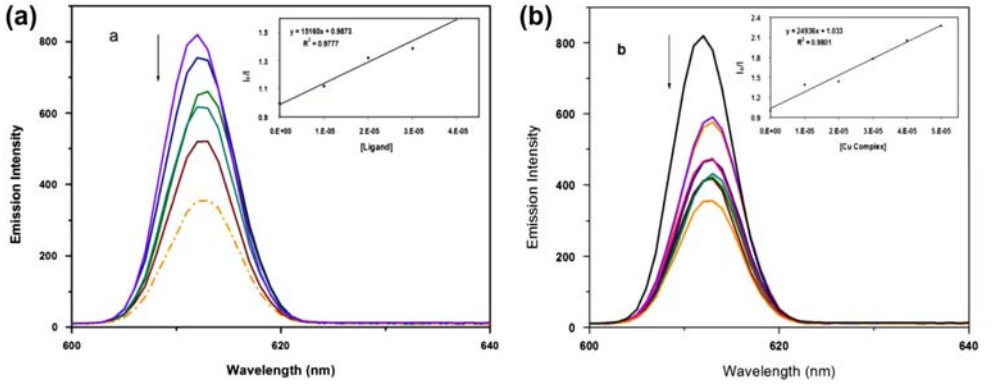

Figure 2. Emission spectra of EB (25 μM) with DNA in the absence and presence of increasing amount of (10–50 μM) (a) L and (b) CuL. The dotted line represents the emission spectrum of EB in the absence of DNA in Tris–HCl buffer containing 5% DMSO.

due to the quenching by solvent. However, on addition of DNA, the fluorescence intensity of EB will be enhanced because of its intercalation into DNA. The fluorescence intensity of EB can be quenched by the addition of another molecule due to a decrease of the binding sites of DNA available for EB [36]. The fluorescence behavior of the EB-DNA adduct in the presence of increasing concentration of compounds is shown in figure 2. The addition of ligand can quench the emission by replacing EB and/or by accepting the excited state electron of the EB through a photo-electron transfer mechanism [37, 38]. In our experiments, increasing concentrations (10, 20, 30, 40, and 50 μM) of the ligand to EB-DNA causes a reduction in emission intensity of ca. 35%, indicating that the ligand binds to DNA. This quenching process is due to accepting the excited state electron of the EB through a photo-electron transfer mechanism. However, on addition of CuL to the EB-DNA adduct causes a reduction in emission intensity of ca. 50%, indicating some EB molecules are exchanged with the CuL and released into solution. This leads to fluorescence quenching of EB. These observations are characteristic of intercalation [39]. The magnitude of the binding strength of the ligand and CuL with CT DNA is determined from the K_{sv} value which is obtained from the linear Stern–Volmer equation (table 3). The apparent binding constant (K_{app}) of CuL was also calculated [$K_{app} = K_{EB}[EB]_{50\%}/[complex]_{50\%}$]. The apparent DNA binding constant of CuL is $5 \times 10^6\ M^{-1}$.

3.7.3. Melting temperature. The binding nature of compounds to DNA and their relative binding strength [40] are predicted by the melting temperature method. The melting temperature (T_m) is the temperature at which the double helix denatures into single strand DNA. Interaction of small molecules with double helix DNA leads to an increase in the T_m value. Intercalation with DNA leads to a difference in the melting temperature of DNA (ΔT_m), while a low value (1–3°C) indicates nonintercalative binding [41]. The melting curves of CT DNA (200 μM) in the presence and absence of both the ligand and CuL (40 μM) are presented in figure S8. The T_m of CT DNA in buffer solution is 58.0 ± 0.5 °C. In the presence of L (40 μM), the T_m of CT DNA increases to 60.0 ± 0.5 °C. This low ΔT_m value implies that the ligand binds DNA through groove binding. However, in the

presence of CuL (40 μM), the T_m of CT DNA increases to 68.0 ± 0.5 °C. Such a high ΔT_m value denotes that CuL binds CT DNA through intercalation.

3.7.4. Viscosity measurements. It is well established that intercalation results in lengthening of DNA, producing an increase in the relative specific viscosity of solution of DNA [42]. In contrast, partial and/or non-classical intercalation bends (or kinks) the DNA helix and reduces its effective length and in turn, its viscosity. On increasing the amount of ligand to CT DNA, the relative viscosity decreases slowly (figure S9). This clearly indicates that the thiazolidine ring of L containing free–NH–group is involved in secondary interactions like H-bonding with DNA, bending or kinking of the DNA helix and decreasing the relative viscosity. Upon increasing the amount of the complex, the relative viscosity of DNA increases steadily and suggests that the complex binds DNA by intercalation.

3.7.5. Cyclic voltammetry. A cyclic voltammetric study of the interaction between CuL and DNA provides a useful complement to spectral studies. The typical CV behavior of CuL in the presence of increasing DNA concentration is shown in figure S10. The voltammogram of CuL shows two anodic peaks ($Ep_{a1} = -0.653$ and $Ep_{a2} = 0.387$ V). The first oxidation peak corresponds to Cu(0)/Cu(I) and the second peak belongs to Cu(I)/Cu(II). Upon reverse scan, the reduction of Cu(II)/Cu(0) occurs at −0.849 V. Potential separation between the anodic and the cathodic waves (ΔE) for Cu(II)/Cu(I) indicates that the process is quasi-reversible. The electrochemical potential of the compound shifts positively when the molecule intercalates into the DNA double helix, and it shifts in a negative direction if the molecule is bound to DNA by an electrostatic interaction [43]. Upon the addition of DNA to CuL, the cathodic peak intensity decreases and the peak potential of both cathodic and anodic peaks are shifted slightly to the positive. The voltammetric current drop in the presence of DNA clearly demonstrates the slow diffusion of the CuL-bound DNA. The anodic and cathodic peak separation potentials become smaller, indicating that the electron transfer process in the complex slows down in the presence of DNA. These results reveal intercalation of CuL with DNA.

3.8. *DNA cleavage studies*

The DNA cleavage mechanism of CuL to pUC19 DNA was investigated by agarose gel electrophoresis. The agarose gel electrophoresis pattern for cleavage of pUC19 DNA by the compounds is given in figure 3. The naturally occurring form of DNA is the supercoiled form (SC). On cleavage, the SC gives open circular relaxed form (Nicked form

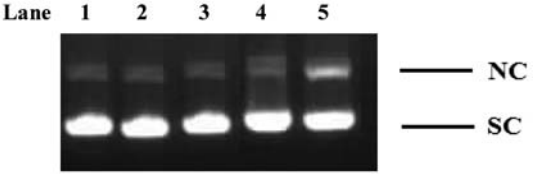

Figure 3. Cleavage of pUC19 plasmid DNA (5 μg) by L and CuL. Lane 1: DNA + H_2O_2; Lane 2: L(40 μM) +DNA; Lane 3: L(40 μM)+DNA + H_2O_2; Lane 4: CuL(40 μM)+DNA; Lane 5: CuL(40 μM)+DNA + H_2O_2.

[NC]). During gel electrophoresis, relatively fast migration is observed for the SC form, whereas for the NC form there is slow migration. In the control experiments, no DNA cleavage is observed when H_2O_2 is present with DNA (lane 1). The ligand (lanes 2 and 3) does not show cleavage activity in the presence and absence of hydrogen peroxide. This indicates that the ligand interacts with DNA through non-intercalation. CuL (lane 4) is inactive in the absence of hydrogen peroxide, whereas in the presence of H_2O_2 (lane 5) Cu(II) species are reduced to Cu(I) species, which binds to DNA with an affinity higher than the Cu(II) species. Thus DNA is made more accessible for the reactive oxygen species (•OH) produced by the Fenton-type reaction resulting in DNA cleavage. This indicates that the CuL complex can cleave the DNA through an oxidative cleavage mechanism.

3.9. *Antioxidant activity (DPPH assay)*

Antioxidants on interaction with DPPH• can either transfer an electron or hydrogen to DPPH•, thus neutralizing its free-radical character. The color of DPPH changes from purple to yellow and its absorbance decreases at 517 nm. The free-radical-scavenging activity of L and CuL towards DPPH• is presented in figure 4(a). The scavenging activity of the ligand is due to the presence of the thiazolidine ring and the phenolic OH. The complex shows higher activity when compared to the ligand, which clearly suggests that the coordination of copper with the thiazolidine ring system increases its capacity to stabilize unpaired electrons and, thereby, to scavenge free radicals. The IC_{50} values of L and CuL are 0.3 and 0.125 mg/mL, respectively.

3.9. *Cytotoxic studies*

The ligand and the CuL were assayed for cytotoxic activity against HCT116 cells by the MTT assay method. The results are shown in figure 4(b). The cells were exposed for a total of 48 h to compare the results of the cell uptake experiments with the cytotoxicity. The IC_{50} values of L and CuL were compared with the thiazole moiety containing compound DAT1 as control [16]. Both compounds show moderate cytotoxic activity against the selected tumor cells. The IC_{50} (concentrations of drug required to inhibit tumor

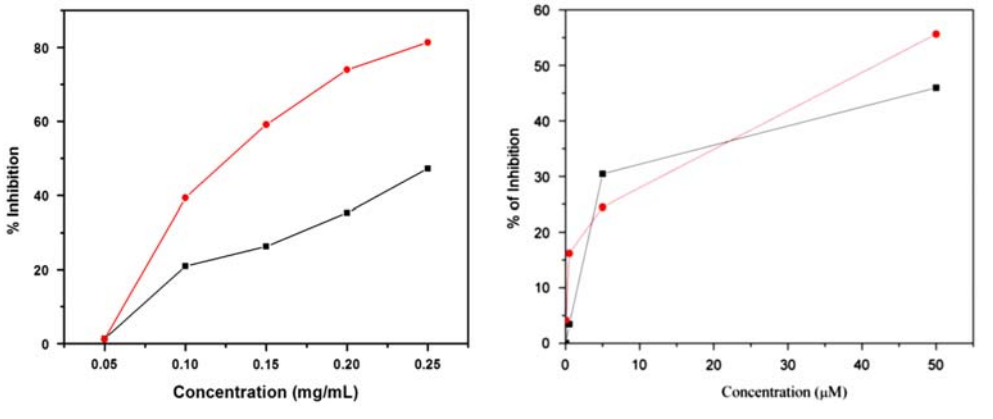

Figure 4. (a) Percentage of inhibition of DPPH radical by (■) L and (●) CuL; (b) HCT116 inhibition capacity of L (■) and CuL (●).

cell growth by 50% of the control) values of L and CuL were 58.08 and 43.66 μM, respectively, in HCT116 cells. So, copper complexation made the ligand more active towards colon cancer cells.

3.11. *Antimicrobial activity*

The ligand and its CuL were tested for inhibitory effects on bacteria, fungi, and yeast. The standard drugs amoxicillin, ampicillin and nystatin were also tested for their activity at the same concentration under conditions similar to that of the test compounds. The results of antibacterial activity indicate that the CuL shows almost equal activity of the standard drug ampicillin against bacterial strains (figure S11). The zone of inhibition of the antimicrobial activities is presented in tables 4 and 5.

The antibacterial effect of the CuL may be due to the contact antibacterial mechanism or the stripping antibacterial mechanism. For the contact antibacterial mechanism, the copper metal combines quickly and tightly with the –SH of pheron in the bacterial body, by which the enzyme needed by the organism loses the activation and the metabolism process was terminated and thus the bacteria were killed. For the stripping antibacterial mechanism, antibacterial ions stripping from antibacterial material react with the protein and nucleic acid of the bacteria. This makes the enzymes of the organism lose activation, resulting in stopping metabolism and death of the bacteria. The antifungal activity revealed that the complex exhibits the highest activity against *Trichoderma harzianum* and lowest to *Aspergillus* (figure S12). The microbial activity of ligand may be due to the presence of the heterocyclic ring, thiazolidine, in the side chain. This thiazolidine ring in the penicillins frame and β-lactam antibiotic family plays a vital role in its action mechanism on the inhibition of the microbial cell wall syntheses [8].

3.12. *SEM analysis*

The effect of the CuL on the surface morphological characteristics of the penicillium species was observed under the scanning electron microscope at a magnification range of 500×, operated at an accelerating voltage of 25 kV. figure 5 shows the SEM images of the

Table 4. Antibacterial activities of L and CuL by well plate method (zone formation in cm).

	Zone of inhibition (in cm) (zone = 0.4 cm)			
Compound	*E. coli*	*Pseudomonous*	*Salmonella Typhi*	*Vibrio*
Ligand	0.8	0.6	0.7	0.5
CuL	1.5	0.9	0.8	1.1
Amoxicillin	1.3	1.3	1.4	1.7
Ampicillin	1.7	1.0	0.8	1.5

Table 5. Inhibition zone (in cm) formed by L and CuL against the growth of fungi.

Compound	*A. Niger*			*Trichoderma*			*Saccharomyces*			*Penicillium*		
Hours	24	48	72	24	48	72	24	48	72	24	48	72
L	0.3	0.4	0.4	0.6	0.7	0.8	0.6	0.8	0.8	0.5	0.6	0.70
CuL	0.8	0.8	0.8	1.0	1.1	1.3	0.8	1.1	1.3	0.8	1.1	1.3
Nystatin	1.3	1.3	1.3	1.3	1.5	1.7	1.2	1.5	1.7	1.1	1.4	1.6

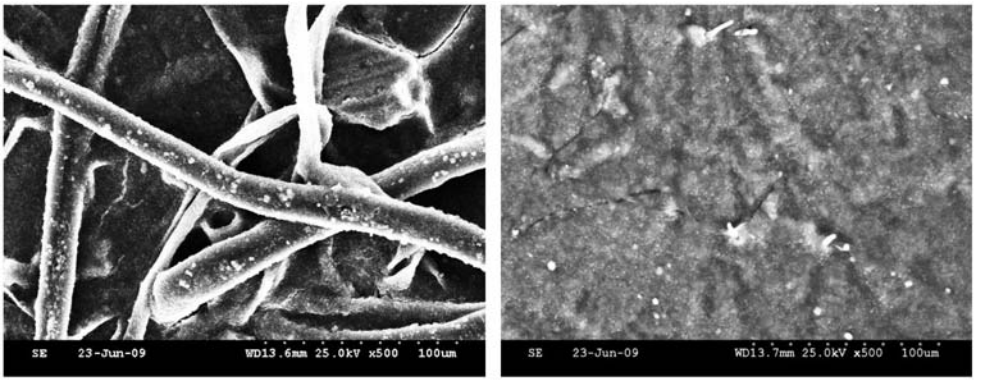

Figure 5. Scanning electron micrographs depicting the effect of metal on the cell morphology and dimensions of penicillium in the absence (a) and presence of CuL (b) at a magnification of 500×.

penicillium species in the presence and absence of the CuL. The thiazolidine ring in the complex exhibits one or more types of tolerance strategies or resistance mechanisms against fungi. The inhibitory effect against growth of penicillium tolerance of metals is based on the ionic species associating with the cell surface or extra cellular polysaccharides, proteins, and chitins [44].

4. Conclusions

The thiazolidine-4-carboxylic acid derivative synthesized by cyclic condensation of D-penicillamine and 3-methoxy salicylaldehyde forms a CuL through the phenolic oxygen, thiazolidine ring nitrogen, and carboxylate oxygen. DNA binding studies reveal that the ligand binds through groove binding, while the complex binds through intercalation. The CuL cleaves DNA through an oxidative cleavage mechanism. CuL shows higher scavenging activity than L. The compounds show moderate cytotoxic activity against selected tumor cells. The CuL shows nearly equal antibacterial activity as that of ampicillin.

Supplementary material

Spectra, TGA/DTA, melting curve, viscosity, and antibacterial activity of the ligand and CuL are embedded in the supplementary material.

Acknowledgements

M.A.N. acknowledges the Department of Science and Technology (DST), New Delhi, India (SR/S1/IC-08/2010) for the financial support. One of the authors, B.A., thanks DST for the fellowship. The authors thank Dr. Balachandran Unni Nair, CLRI, Chennai, for help in DNA cleavage studies. The authors are very much thankful to the Editor for valuable suggestions and for the modification of the manuscript.

References

[1] X. Fernandez, R. Fellous, L. Lizzani-Cuvelier, M. Loiseau, E. Dunach. *Tetrahedron Lett.*, **42**, 1519 (2001).
[2] M. Gosálvez. *Abstr., Proc. Am. Assoc. Cancer Res. New Orleans*, **20**, 17 (1979).

[3] A.J. Lucke, J.D.A. Tyndall, Y. Singh, D.P. Fairlie. *J. Mol. Graphics Modell.*, **21**, 341 (2003).
[4] B.A.Abdel-Rahman El-Gazzar, Alaa-El-Din M. Gaafar, S.A. Aly. *J. Sulfur Chem.*, **29**, 549 (2008).
[5] M. Gosálvez, L. Pezzi, C. Vivero. *Biochem. Soc. Trans.*, **6**, 659 (1978).
[6] A. Brugarolas, M. Gosálvez. *Lancet*, **316**, 68 (1980).
[7] M.S. Nair, M.A. Neelakantan. *J. Ind. Chem. Soc.*, **77**, 373 (2000).
[8] K. Dey, S. Sarkar, S. Mukhopadhyay, S. Biswas, B.B. Bhaumik. *J. Coord. Chem.*, **59**, 565 (2006).
[9] C.A. Bolos, K.T. Papazisis, A.H. Kortsaris, S. Voyatzi, D. Zambouli, D.A. Kyriakidis. *J. Inorg. Biochem.*, **88**, 25 (2002).
[10] L.G. Craig, W.F. Phillips, M. Burachik. *Biochemistry*, **8**, 2348 (1969).
[11] E.D. Harris. Copper in Human and Animal Health. In *Trace Elements in Health*, J. Rose (Ed.), pp. 44–73, Butterworths, London (1983).
[12] D.D. Perrin, W.L.F. Armarego, D.R. Perrin. *Purification of Laboratory Chemicals*, Pergamon Press, Oxford (1980).
[13] A. Wolfe, G.H. Shimer, T. Meehan. *Biochemistry*, **26**, 6392 (1987).
[14] O. Stern, M. Volmer. *Z. Phys.*, **20**, 183 (1919).
[15] M. Lee, A.L. Rhodes, M.D. Wyatt, S. Forrow, J.A. Hartley. *Biochemistry*, **32**, 4237 (1993).
[16] S.A. Thomas, R. Thamkachy, B. Ashokan, R.J. Komalam, K.V. Sreerekha, A. Bharathan, T.R. Santhoshkumar, K.N. Rajasekharan, S. Sengupta. *J. Pharmacol. Exp. Ther.*, **341**, 718 (2012).
[17] M.J. Pelczar, E.C.S. Chan, N.R. Kreig. *Microbiology*, Blackwell Science, New York, NY (1998).
[18] C. Perez, M. Pauli, P. Bazerque. *Acta Biol. Med. Exp.*, **15**, 113 (1990).
[19] W.J. Geary. *Coord. Chem. Rev.*, **7**, 81 (1971).
[20] K. Nakamoto. *Infrared Spectra of Inorganic and Coordination Compounds, Part B*, 5th Edn Edn, Wiley Interscience, New York, NY (1997).
[21] J.R. Ferraro. *Low-Frequency Vibrations of Inorganic and Coordination Compounds*, Plenum Press, New York, NY (1971).
[22] R.B. Martin, R. Mathur. *J. Am. Chem. Soc.*, **87**, 1065 (1965).
[23] G. Asgedom, A. Sreedhara, J. Kivikoski, E. Kolehmainen, C.P. Rao. *J. Chem. Soc., Dalton Trans.*, 93 (1996).
[24] B. Harikumar, M.R.P. Kurup, T.N. Jayaprakash. *Transition Met. Chem.*, **22**, 507 (1997).
[25] R.C. Chikate, A.R. Belapure, S.B. Padhye, D.X. West. *Polyhedron*, **24**, 889 (2005).
[26] A.K. Patra, T. Bhowmick, S. Roy, S. Ramakumar, A.R. Chakravarty. *Inorg. Chem.*, **48**, 2932 (2009).
[27] A. Matsumoto, T. Fukumoto, H. Adachi, H. Watarai. *Anal. Chim. Acta*, **390**, 193 (1999).
[28] W.A. Alves, G. Cerchiaro, A.P. Filho, D.M. Tomazela, M.N. Eberlin, A.C. Ferreira. *Inorg. Chim. Acta*, **358**, 3581 (2005).
[29] S. Neidle. *Nat. Prod. Rep.*, **18**, 291 (2001).
[30] S. Rajalakshmi, T. Weyhermüller, A.J. Freddy, H.R. Vasanthi, B.U. Nair. *Eur. J. Med. Chem.*, **46**, 608 (2011).
[31] L.S. Lerman. *J. Mol. Biol.*, **3**, 18 (1961).
[32] B.C. Jonathan. *Biopolymers*, **44**, 201 (1997).
[33] S.H. Cui, M. Jiang, Y.T. Li, Z.Y. Wu, X.W. Li. *J. Coord. Chem.*, **64**, 4209 (2011).
[34] H.L. Wu, X. Huang, B. Liu, F. Kou, F. Jia, J. Yuan, Y. Bai. *J. Coord. Chem.*, **64**, 4383 (2011).
[35] Y. Mei, J.J. Zhou, H. Zhou, Z.Q. Pan. *J. Coord. Chem.*, **65**, 643 (2012).
[36] B.C. Baguley, M. Le Bret. *Biochemistry*, **23**, 937 (1984).
[37] B. Selvakumar, V. Rajendiran, P.U. Maheswari, H. Stoeckli-Evans, M. Palaniandavar. *J. Inorg. Biochem.*, **100**, 316 (2006).
[38] J.K. Barton, J.M. Goldberg, C.V. Kumar, N.J. Turro. *J. Am. Chem. Soc.*, **108**, 2081 (1986).
[39] C.V. Kumar, J.K. Barton, M.J. Turro. *J. Am. Chem. Soc.*, **107**, 5518 (1985).
[40] S.D. Choi, M.S. Kim, S.K. Kim, P. Lincoln, E. Tuite, B. Norden. *Biochemistry*, **36**, 214 (1997).
[41] P.U. Maheswari, M. Palaniandavar. *J. Inorg. Biochem.*, **98**, 219 (2004).
[42] Z. Bin, L. Yan, T. Xiaoning, X. Yinhua, X. Gang. *J. Rare Earths*, **28**, 442 (2010).
[43] A.J. Bard, L.R. Faulkner. *Electrochemical Methods*, Wiley, New York, NY (1980).
[44] B. Volesky. Biosorption and Biosorbents. In *Biosorption of Heavy Metals*, B. Volesky (Ed.), pp. 3–6, CRC Press, Boston (1990).